CHEMISTRY OF MATERIALS

Article

pubs.acs.org/cm

Insights on the Mechanism of Na-Ion Storage in Soft Carbon Anode

Zelang Jian,[†,⊥] Clement Bommier,[†,⊥] Langli Luo,[‡] Zhifei Li,[†] Wentao Wang,[†] Chongmin Wang,[*,‡] P. Alex Greaney,[*,§] and Xiulei Ji[*,†]

[†]Department of Chemistry, Oregon State University, Corvallis, Oregon, 97331, United States

[‡]Environmental Molecular Sciences Laboratory, Pacific Northwest National Laboratory, Richland, Washington 99352, United States

[§]Materials Science and Engineering Program, University of California, Riverside, California, 92521, United States

Supporting Information

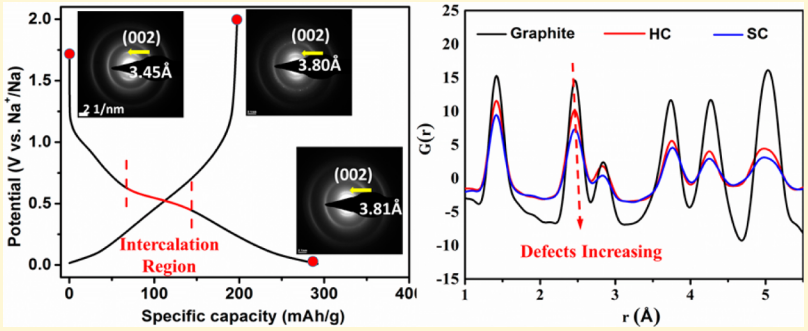

ABSTRACT: Graphite is the commercial anode for lithium-ion batteries; however, it fails to extend its success to sodium-ion batteries. Recently, we demonstrated that a low-cost amorphous carbon—soft carbon exhibits remarkable rate performance and stable cycling life of Na-ion storage. However, its Na-ion storage mechanism has remained elusive, which has plagued further development of such carbon anodes. Here, we remedy this shortfall by presenting the results from an integrated set of experimental and computational studies that, for the first time, reveal the storage mechanism for soft carbon. We find that sodium ions intercalate into graphenic layers, leading to an irreversible quasi-plateau at ∼0.5 V versus Na^+/Na as well as an irreversible expansion seen by in situ transmission electron microscopy (TEM) and X-ray diffraction (XRD). Such a high-potential plateau is correlated to the defective local structure inside the turbostratic stacking of soft carbon and the associated high-binding energies with Na ions, suggesting a trapping mechanism. On the other hand, soft carbon exhibits long sloping regions above and below the quasi-plateau during the first sodiation, where the sloping regions present highly reversible behavior. It is attributed to the more defects contained by soft carbon revealed by neutron total scattering and the associated pair distribution function studies.

INTRODUCTION

The critical role of energy storage is by now self-evident: they are indispensable for the proliferation of renewable energy installation. Considering the abundance of sodium resources, sodium-ion batteries (NIBs) are poised as the sustainable electrochemical energy storage (EES) solution.[1−6] However, several technical challenges still remain to be addressed before the commercialization of NIBs, with the anode being one of them. Graphite has been employed as the anode for commercial lithium-ion batteries (LIBs) since 1991.[7] Recently, Jian et al. first reported that graphite can be used as a promising anode for potassium-ion batteries (KIBs) with a high reversible capacity of 273 mAh/g.[8] It is thermodynamically favorable to form the stage-one Li- or K-graphite intercalation compounds (GICs), that is, LiC_6 and KC_8, respectively.[7−12] However, the most Na-rich GIC prepared to date is NaC_{64} with a capacity of only 35 mAh/g unless solvent molecules are coinserted or unless expanded graphite is used.[13−15] The failure of graphite in storing Na is driven by thermodynamics,[16] where the free-energy difference between the hypothetical Na-GIC, graphite, and sodium metal is not negative, and thus, Na-plating would occur before Na-intercalation into graphite. Therefore, alternative anode materials are demanded. One family of candidates is nongraphitic carbon, which comes in the forms of "hard carbon" or "soft carbon". The former cannot be converted to graphite even when being annealed at 2500 °C, while the latter can. The disordered structures of these carbons render them more amenable in Na-ion storage than graphite.[17−19]

Hard carbon as an NIB anode was first reported in 2000 by Stevens and Dahn with a high reversible capacity of ∼300 mAh/g.[20] While it has gathered much attention because of its ease of preparation from biomass sources and good performances, a few caveats exist.[21−23] The high capacity of hard carbon in its potential profiles comprises a high-potential sloping region followed by a low-potential plateau region (a typical

Received: December 27, 2016
Revised: February 9, 2017
Published: February 27, 2017

DOI: 10.1021/acs.chemmater.6b05474
Chem. Mater. 2017, 29, 2314−2320

sodiation/desodiation potential profile of hard carbon is shown in Figure S1). The low-potential plateau, close to 0 V versus Na^+/Na, accounts for more than half of its capacity. However, such a low sodiation potential causes three significant concerns.[24] First, the low potential is associated with the possibility of Na-metal plating, which, if it occurs, may cause battery thermal runaway. Second, the low-potential plateau is sensitive to polarization, which causes low capacities at higher current rates.[25] Third, the low potential may result in electrolyte degradation, which would limit the cycling life.

In contrast to hard carbon, soft carbon is typically derived from aromatic masses, such as pitch or tar, or from petroleum or coal refinement or plastics with low oxygen contents.[26,27] Unlike hard carbons, soft carbon demonstrates a generally sloping potential profile during sodiation and desodiation, which lacks the low-potential plateau.[18,28] As a result, the major trunk of its reversible capacity is from the potentials well above where Na plating may occur, thereby alleviating the concerns of dendrite formation, polarization, and high reactivity. Thus, the sloping profile enables the soft carbon to have a better rate capability and a long cycling life. Interestingly, the distinct sloping sodiation profile of soft carbon differentiates from that of hard carbon because both materials exhibit nearly identical X-ray diffraction (XRD) patterns and Raman spectra. The disparity of the electrochemical properties between hard and soft carbon must be attributed to their unique atomic and nanometric structures. As shown in Figure 1a and b, the graphenic layers in hard carbon are very much curved and are not aligned, whereas the graphenic layers in soft carbon exhibit less curvature and are much better aligned.

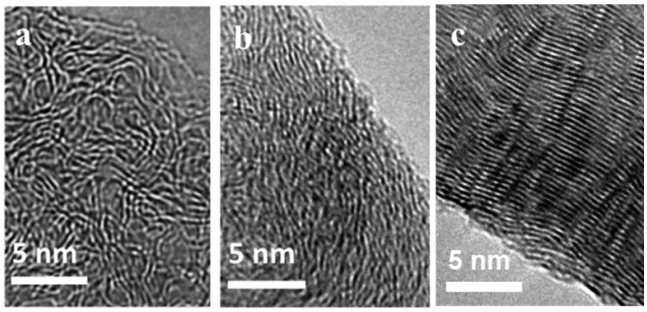

Figure 1. High-resolution transmission electron microscopy (HRTEM) images of (a) hard carbon, (b) SC-900, and (c) SC-1600.

Recently, we investigated the Na-ion storage properties of a soft carbon derived from an organic molecular solid of perylene tetracarboxylic dianhydride (PTCDA), an inexpensive red pigment (see its unit cell in Figure S2). We observed high reversible capacity values, that is, 200 mAh/g, high rate capability, and stable cycling life from this soft carbon as an NIB anode. Interestingly, the annealed soft carbon exhibits capacity values inversely proportional to the annealing temperatures. Upon annealing at 1600 °C, the resulting soft carbon displays a quasi-graphitic structure under transmission electron microscopy (TEM), as shown in Figure 1c, which reveals the graphitizable nature of this carbon. Thereafter, we have been working on this carbon as a model soft carbon to elucidate its mechanism of Na-ion storage.

While the Na-ion storage mechanism for hard carbon is still under debate, a lack of any proposed mechanisms for Na-ion storage in soft carbon remains. As for the sloping and plateau regions for the hard carbon's potential profiles, in their pioneering work, Stevens and Dahn proposed the structure–capacity relationships, where the sloping region is assigned to the Na intercalation inside turbostratic nanodomains and where the plateau region is attributed to the nanoplating inside the voids of hard carbon.[20] The assignments are on the basis of the well-known structural model of hard carbon: the card-house model raised in 1951 by Franklin, who also conducted her well-known DNA crystallography work after studying hard carbon.[29] In the card-house model, short turbostratic nanodomains with large (002) *d*-spacing are randomly oriented and cross-linked, forming a molecular sieve framework with a relatively low density of ~1.5–1.6 g/cc in contrast to 2.2 g/cc for bulk graphite.

In terms of the structure–capacity assignments for the sloping and plateau regions of hard carbon, recently, there have been some different voices. Notably, Ding et al.[30] and Komaba et al.[31] attribute the low-potential plateau to the intercalation of Na ions into the turbostratic nanodomains as they observed that the XRD (002) peak shifts to a lower angle upon Na insertion at the low-potential range. Such an intercalation–plateau correlation has been supported by our recent results, where we increased the (002) *d*-spacing of hard carbon by doping PO_x species, which greatly enhances the capacity contribution from the plateau region.[32] Typically, a potential plateau is caused by a two-phase redox reaction, in which there is no significant concentration variance across the phase boundary.[33,34] For the sloping region, our recent neutron total scattering and the associated pair distribution function

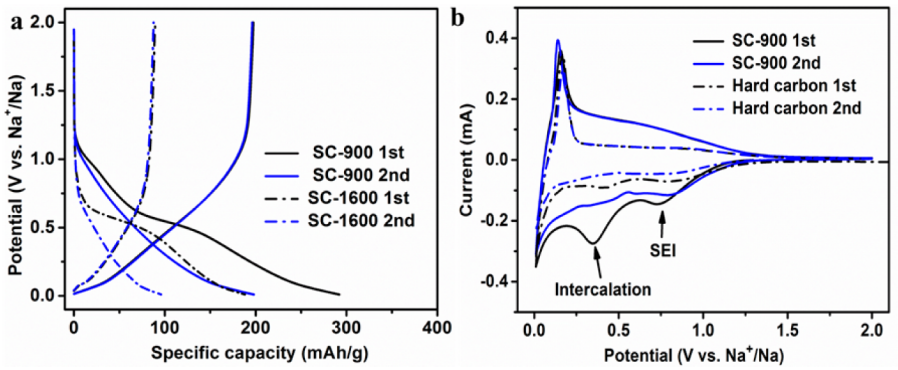

Figure 2. (a) The first two cycles of sodiation/desodiation potential profiles of SC-900 and SC-1600 at 20 mA/g; (b) CV curves of SC-900 and hard carbon with a scan rate of 0.1 mV/s.

DOI: 10.1021/acs.chemmater.6b05474
Chem. Mater. 2017, 29, 2314–2320

(PDF) studies reveal that removal or addition of defects decreases or increases sloping capacity, respectively, thus suggesting a defect−slope correlation.[32,35] The earlier postulated mechanism appears credible for hard carbon; the question is whether such insights can be extended to the mechanism of Na-ion storage in soft carbon.

RESULTS AND DISCUSSION

Figure 2a shows the sodiation/desodiation potential profiles of two soft carbon samples annealed at 900 and 1600 °C. During the first sodiation, there is a quasi-potential plateau, the region between two inflection points, centered at ∼0.55 V for both samples, where all potentials are referred to Na^+/Na in this study. However, this plateau vanished in the following desodiation. This irreversible phenomenon is observed in the first cyclic voltammetry (CV) cycle as well, where the middle cathodic peak at ∼0.35 V disappeared in the following anodic scan (Figure 2b).

We hypothesize that the irreversible plateau is due to the intercalation of Na ions between graphenic layers. The hard carbon does not exhibit this irreversible behavior at the same potential (Figure 2b dashed profiles). For carbon anodes, irreversibility is often attributed to the formation of solid electrolyte interphase (SEI). The primary determinant of SEI formation is the specific surface area of the electrodes. The soft carbon samples investigated in this study have a Brunauer−Emmett−Teller (BET) specific surface area below 30 m^2/g (Figure S3), which is slightly lower than that of the hard carbon. Furthermore, all electrochemical conditions are identical when testing soft and hard carbon anodes. This irreversible plateau (peak) only belonging to soft carbon cannot be a function of electrolyte decomposition.

As evidence of Na-ion intercalation in soft carbon, our prior ex situ TEM observation had shown a large degree of (002) lattice expansion of soft carbon.[18] Ex situ XRD results also confirm the expansion irreversible (Figure S4), where the (002) peak shifts from 2θ 25° to 2θ 21° upon the first sodiation, corresponding to an expansion from 3.6 to 4.2 Å, but the following desodiation cannot shift this peak back. The irreversible expansion was confirmed by in situ TEM studies. Figure S5 shows the schematic of the in situ TEM cell setup. We took the selected area electron diffraction (SAED) patterns of SC-900, which depicts that the (002) *d*-spacing increases from 3.45 to 3.81 Å upon the first sodiation (Figure 3a, b). However, the *d*-spacing does not decrease to its original value in the following desodiation (Figure 3c). Even after the second desodiation, the *d*-spacing remains around 3.8 Å (Figure 3d, e). Similar in situ TEM studies were carried out on the nearly graphitic sample of SC-1600 (Figure S6), where the *d*-spacing gradually increases to 3.95 Å upon sodiation. The local expansion inside SC-1600 has resulted in electrode-particle swelling, a macroscopic expansion, as shown in a video in the Supporting Information.

The XRD and TEM results indicate that insertion of Na ions dilates the turbostratic nanodomains, where some Na ions as spacers are permanently trapped in the structure, thus causing the irreversible plateau. To confirm this trapping mechanism, we collected Na elemental mapping from cross sections of the fully desodiated soft carbon particles, where the cross sections were prepared by focus ion beam (FIB) milling. Figure 4 shows a cross section and the corresponding energy-dispersive X-ray (EDX) elemental mapping of C and Na. It is evident that after complete desodiation to a cutoff voltage of 2 V, concentrated

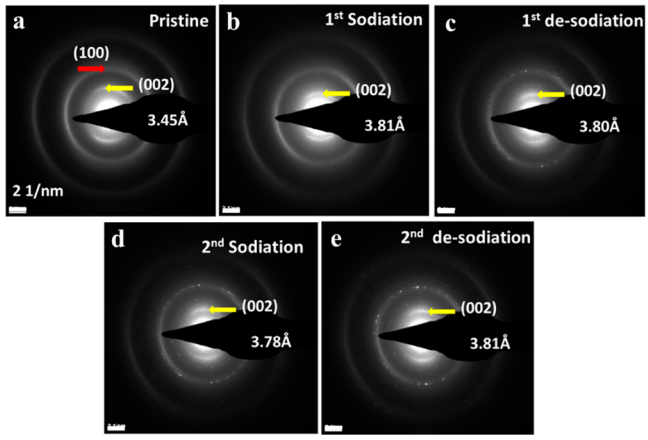

Figure 3. In situ TEM SAED at different states of charge of SC-900 sample.

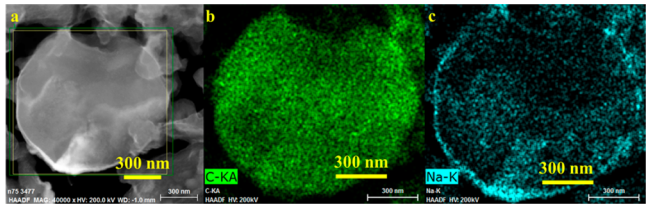

Figure 4. TEM and EDX imaging of fully desodiated SC-900 after the first cycle. (a) TEM image of a cross section of a soft carbon electrode particle, (b) carbon elemental mapping, and (c) Na elemental mapping.

Na exists trapped inside soft carbon particles as well as on the particle surface, where the surface Na-containing layer is attributed to the SEI formation.

We assign the quasi-plateau in the first sodiation profile to the irreversible intercalation. However, it is intriguing to compare this high-potential intercalation plateau of soft carbon to that of hard carbon, which is at low potentials and which is highly reversible.[13] The question is why the intercalation in soft carbon takes place at this high potential. A higher potential in carbon/Na half-cells suggests a greater Na-ion binding energy for the intercalation sites in soft carbon than the counterpart sites in hard carbon. Typically, defect sites bind intercalant metal ions more strongly; thus, it is necessary to investigate whether this soft carbon contains a more defective local structure. To investigate the local order, we conducted neutron total scattering and the associated PDF studies for SC-900 and hard carbon for comparison. The PDF results come from the following equation:

$$G(r) = \frac{2}{\pi}\int_0^\infty Q[S(Q) - 1]\sin(Qr)\mathrm{d}Q \quad (1)$$

where $S(Q)$ is the structure function comprising both Bragg and diffuse scattering, and Q is the scattering vector.[36] In $G(r)$, the peak positions (r) correspond to real-space distances between an arbitrarily selected atom and its neighbors averaged over all atoms contained in the sample. The peak integral is proportional to the coordination numbers of the correlating atom pairs around a certain distance, where the lower amplitude indicates more defects (or curvatures) along the *ab* graphenic planes. As a reference sample, graphite gives rise to peaks with amplitude much higher than that of hard carbon and soft carbon.[37] Graphite also exhibits long coherence lengths,

DOI: 10.1021/acs.chemmater.6b05474
Chem. Mater. 2017, 29, 2314−2320

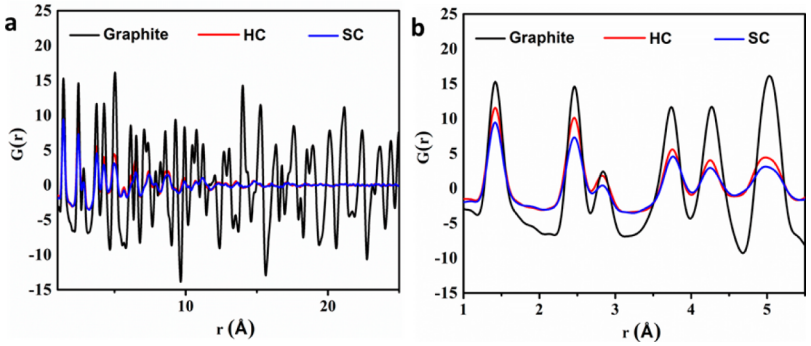

Figure 5. PDF results of neutron total scattering of soft carbon, hard carbon, and graphite: (a) a long-range profile and (b) the expanded short-range profile.

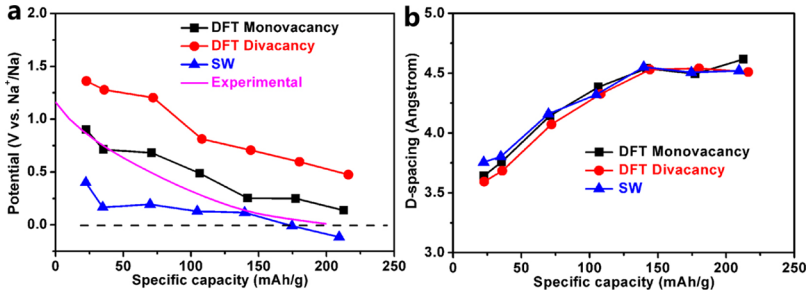

Figure 6. (a) Simulated potential profiles from the DFT simulation using various defective bilayers as compared to the experimental second sodiation profile obtained in GITT studies, where the relaxed points are connected to form this curve. The capacity was increased by progressively adding Na atoms. (b) Calculated average *d*-spacing from the DFT simulation.

which is suggested by the fact that its peaks do not diminish over the full range of length in the PDF profile. In contrast, the peaks' amplitude of hard carbon and soft carbon decreases rapidly along *r* values, where their coherence lengths are no longer than 15 Å (Figure 5a). Most importantly, by comparing with hard carbon, soft carbon shows lower amplitude of peaks, as shown in Figure 5b, indicative of soft carbon's more defective local structure than that of hard carbon. This sheds light on why the overall sodiation potential of SC-900 is higher than that of hard carbon. Intercalation of Na ions through more defective turbostratic domains may result in a plateau of higher potentials than through less defective domains in hard carbon. Furthermore, considering the longer diffusion paths of Na ions in soft carbon's more defective turbostratic domains that are much larger than the nanodomains in hard carbon, it is more likely that Na ions are trapped by defect sites deep in the particles of soft carbon (Figure 4c).

On the other hand, soft carbon's being more defective than hard carbon may provide insights on the higher slope capacity for soft carbon than for hard carbon. When we subtract the plateau capacity from the total sodiation capacity of SC-900, the first slope sodiation capacity is 205 mAh/g, and in the following desodiation, the slope capacity is ∼195 mAh/g, being highly reversible (Figure 2a). This reversible desodiation slope capacity is significantly higher than the reversible slope capacity of hard carbon of 150 mAh/g.[20] The higher slope capacity of soft carbon should be ascribed to the more defects in carbon local structures. Moreover, when we compare the capacity between SC-900 and SC-1600, it is evident that a higher annealing temperature decreases the slope capacity, which is in accordance with the observation on the trend of annealed hard carbon samples.[35] As high-temperature annealing would remove some defects, this further supports the assignment of defect−slope correlation for both hard carbon and soft carbon.

To further understand the nature of Na-ion binding in local carbon structural sites, we conducted density functional theory (DFT) analysis. To represent the soft carbon's structure for simulation, we tested three bilayer graphenic structures. One contains a monovacancy in one of the bilayers; one has a Stone−Wales defect in one of the bilayers; one comprises a pair of aligned monovacancy on adjacent sheets, where for brevity we refer to this situation as a divacancy, although the two vacancies are not in the same graphene sheet. The bilayers were set to have an interlayer distance of 3.56 Å, which is selected according to the average (002) *d*-spacing value of SC-900. We allow the bilayers to accommodate a range of different Na-ion concentrations, which correlates to the sodiation capacity observed in a C/Na half-cell. The simulated voltage can be obtained through the following equation:

$$e^{-}V = \frac{(E_{\text{carbon+Na}} - E_{\text{carbon}}) - xE_{\text{Na}}}{x} \quad (2)$$

where V is the theoretical potential of a half-cell; $E_{\text{carbon+Na}}$ is the free energy of the carbon bilayer containing Na atoms in its relaxed state; E_{carbon} is the free-energy term of the carbon bilayer in its relaxed state; E_{Na} represents the energy needed to displace one Na atom from Na metal of the body centered cubic (BCC) structure; and x is the number of inserted Na ions. We do not consider the solvation or desolvation processes of the Na ions as the energy terms of these processes cancel out in the whole system of a half-cell, and we assume that electrolyte solvent molecules are not cointercalated with Na ions into the carbon structures.

In these calculations, the first inserted Na ions bind preferentially at the defect site, and the subsequent inserted

DOI: 10.1021/acs.chemmater.6b05474
Chem. Mater. 2017, 29, 2314−2320

Na ions/atoms bind to pristine parts of the graphenic sheet in the vicinity. The energies of the sodium insertion as a function of different capacity values are plotted in Figure 6. These reveal the surprising result that defects in the graphene affect not just the energy of Na binding directly to the defect but also the energy of Na intercalation into regions vicinal to the defect. The different types of defects provide different affinities for Na storage, with higher-energy defects that are more disruptive to the carbon structure having the stronger effect on intercalation energy (Figure 6a). The divacancy defect leads to high voltages, which goes from 1.36 to 0.48 V as the Na concentration increases from an equivalent capacity of 20 mAh/g to 210 mAh/g. The potential profile from the monovacancy defect is much closer to that of the reversible experimental sodiation potential with the voltage going from 0.90 to 0.13 V with a similar increase in Na concentration. This profile was obtained by galvanostatic intermittent titration technique (GITT), where a constant current at 20 mA/g is applied for 0.5 h before the cell rests at open-circuit voltage (OCV) for 1 h (Figure S7). In contrast, the Stone−Wales defected bilayer has the lowest overall voltage, well below that of the experimental curve. At an equivalent capacity of 20 mAh/g, the voltage is 0.40 and drops into the negative range somewhere between the capacities of 140 mAh/g and 170 mAh/g. Comparing the three different structures, the most defected structure has the highest overall voltage, as the defect sites allow for greater electron transfer from the Na atoms to the graphene structure, thus leading to more ionic binding interactions with the Na atoms. However, in the case of the Stone−Wales defect, the electron transfer to the carbon structure was not as great, and as a result, it could not favorably intercalate large numbers of Na atoms. This problem would have been exacerbated with a pristine bilayer structure, as the degree of electron transfer would have been even smaller, and intercalation would not have been possible.

Comparing the simulation results to the experimental results, we see that the simulated monovacancy voltage profile matches that of the half-cell well. It is possible that this very nice match is a coincidence as soft carbon is likely to contain a mixture of different types of point defects. However, the results do speak to the general trend of intercalation in defective turbostratic nanodomains. Moreover, these results show that there are some defects that provide very strong Na binding and so could be responsible for irreversible capture of Na on the first sodiation cycle.

In the DFT calculations, Na-ion intercalation between bilayers also leads to progressive bilayer expansion mirroring that observed in the ex situ XRD and in situ TEM measurements. The highest *d*-spacing from the DFT simulation of the bilayers is around 4.5 Å, whereas the one from the ex situ experiment reaches a maximum of only 4.2 Å. DFT calculations of Na intercalated into the central gallery of a stack of four graphene sheets has a reduced *d*-spacing of ∼4.2 Å because of the additional interactions between the next nearest graphene layers.

CONCLUSION

On the basis of the earlier mentioned experimental and simulation results, we hope to bring the following insights on the structure−capacity correlation, the first of its kind, for Na-ion storage in soft carbon anode. First, the more defective local structure of soft carbon explains its overall higher sodiation potential than that of hard carbon, particularly the higher potential of the quasi-plateau than the plateau exhibited by hard carbon. Second, when Na ions intercalate soft carbon's turbostratic domains, local as well as macroscopic structural expansion takes place, and such expansion is irreversible, leaving some Na ions trapped in the intercalated sites. Third, the irreversible quasi-plateau in the first sodiation should be assigned to the irreversible structural expansion caused by intercalation. Fourth, such intercalation irreversibility may have to do with the large Na-ion binding energy in the compact turbostratic domains of soft carbon. Fifth, soft carbon exhibits higher reversible slope capacity than hard carbon, which is attributed to its more defective local structure. These insights presented may help guide the community to synthesize more advanced soft carbon anodes for Na-ion batteries, particularly for power battery applications. To reflect on what we have learned in planning for future studies, an ideal soft carbon anode for Na-ion batteries should exhibit large specific capacity values, excellent rate capability, long cycling life, and high first-cycle Coulombic efficiency. At the current stage, encouraging results of the rate capability and cycling life of soft carbon have been demonstrated, as reported by Luo et al.[18] In this study, we have looked into Na-ion storage mechanism in soft carbon, which, to a large extent, reveals the structure−capacity correlation as well as the causality for the low first-cycle Coulombic efficiency. It appears to us that the reversible capacity of soft carbon depends on the reversible binding of Na ions with local defects, that is, vacancies on sp^2 graphenic layers, as uncovered in the neutron total scattering and PDF studies on both soft carbon and hard carbon. To further enhance the capacity, a hypothesis for future studies is to increase the number of local defects for soft carbon. Nevertheless, attention must be paid to the average (002) *d*-spacing of such more defective soft carbon because if the *d*-spacing is too narrow, it is likely that more Na ions would be trapped during the irreversible expansion of the structure. To this end, organic solid precursors with intrinsically large *d*-spacing values may be worthy of investigation, where the preparation should be coupled by carefully selected reaction conditions, such as heating rates and inert gas flow rates during pyrolysis.

METHODS

Experimental Section. Hard carbon was obtained by pyrolyzing sucrose under Ar at 1100 °C for 5 h. Prior to being annealed, sucrose was dehydrated by heating at 180 °C for 24 h. Soft carbon was obtained by pyrolyzing PTCDA under Ar at 900 or 1600 °C for 5 h. The obtained soft carbons were named as SC-900 and SC-1600, respectively, according to the annealing temperature.

The graphitic layer distance of samples was analyzed by powder XRD with Cu Kα radiation at 40 kV and 40 mA (Rigaku). The specific surface area was calculated by the BET method using the adsorption branch of N_2 sorption isotherms. The structure of samples was examined by an FEI Titan 80-300 TEM, and neutron total scattering at the Nanoscale Ordered Materials Diffractometer (NOMAD, Spallation Neutron Source, at Oak Ridge National Laboratory). The neutron samples were loaded into quartz capillaries for testing. The in situ TEM of the sodiation and desodiation of soft carbon (both SC-900 and SC-1600 samples) was carried out using an open-cell configuration (see Supporting Information). The soft carbon was loaded on a Pt rod, which is fixed on one side of the TEM holder (Nanofactory STM). Sodium metal was loaded on a W rod, which is navigated by the piezoelectric system on the other side of the holder. Sodium metal is driven to contact the

DOI: 10.1021/acs.chemmater.6b05474
Chem. Mater. 2017, 29, 2314−2320

soft carbon. The sodium oxide layer on sodium metal surface serves as electrolyte. To drive Na-ion diffusion through Na_2O, an overpotential of 3 V was applied on soft carbon against the Na metal to sodiate the soft carbon. The microstructural changes were recorded using a charge-coupled device (CCD) attached to the TEM.

The working electrodes were prepared by mixing 80 wt % active material, 10 wt % carbon additive, and 10 wt % polyvinylidene fluoride (PVdF) as the binder. The obtained homogeneous slurry was evenly coated onto Cu foil and was dried at 100 °C for 8 h under vacuum. The mass loading was around 2 mg/cm^2. Sodium foil was used as a counter and glass fiber paper was employed as a separator. The electrolyte was 0.8 mol/L $NaPF_6$ in ethylene carbonate and diethyl carbonate (EC:DEC = 1:1 by volume). CR2032 coin cells were fabricated in an Ar-filled glovebox. The electrochemical measurements were performed on an Arbin BT2000 system at room temperature, where the voltage range was from 0.01 to 2 V versus Na^+/Na. GITT with a constant current at 20 mA/g is applied for 0.5 h before the cell rests at open-circuit voltage (OCV) for 1 h.

Computational Section. Theoretical calculations were performed using the Vienna ab initio simulation package (VASP)[38−40] with projector augmented wave (PAW) pseudopotentials[41,42] with general gradient approximation (GGA) and the Perdew−Burke−Ernzerhof (PBE) exchange-correlation functional.[43] Additionally, the DFT-D3 method[44,45] was used to account for the long-range van der Waals forces present within the system. For the computational simulation, an energy cutoff of 500 eV and a 2 × 2 × 2 Monkhorst−Pack[46] KPOINT scheme were used for the brillouin zone integration.

The graphene structures were simulated defective bilayers comprising two 4 × 4 graphene sheets arranged in an AB stacking configuration. The types of defects included in the bilayers include monovacancy, divacancy, and Stone−Wales vacancy. The bilayers were ionically relaxed until the force present was less than 0.01 eV/Å. Once the systems were ionically relaxed, static energy calculations were performed on the carbon−Na system and on the carbon substrate to obtain the difference in energy between the two systems. Additionally, the energy of a Na atom in a BCC unit cell was found to be −1.31 eV/atom, where the value was used when performing the calculations to obtain the simulated voltage profile.

■ ASSOCIATED CONTENT

Supporting Information

The Supporting Information is available free of charge on the ACS Publications website at DOI: 10.1021/acs.chemmater.6b05474.

Sodation/desodiation profile of Na ions in hard carbon, PTCDA structure, schematic diagram of in situ TEM of SC-1600, ex situ XRD patterns of SC-900, BET results, and GITT profile of SC-900 are included
(PDF)

Electrode-particle swelling
(ZIP)

■ AUTHOR INFORMATION

Corresponding Authors

*E-mail: david.ji@oregonstate.edu.
*E-mail: Chongmin.Wang@pnnl.gov.
*E-mail: agreaney@engr.ucr.edu.

ORCID

Xiulei Ji: 0000-0002-4649-9594

Author Contributions

⊥Zelang Jian and Clement Bommier equally contributed to this work.

Notes

The authors declare no competing financial interest.

■ ACKNOWLEDGMENTS

X. J. and P. A. G. thank the financial support from the U.S. National Science Foundation, award Number 1507391. C. M. W. is grateful to the support from the U.S. Department of Energy, award number DE-AR0000297TDD. C. M. W is supported by the Assistant Secretary for Energy Efficiency and Renewable Energy, Office of Vehicle Technologies of the U.S. Department of Energy under Contract No. DE-AC02-05CH11231, Subcontract No. 6951379 under the advanced Battery Materials Research (BMR) program. The in situ TEM was conducted in the William R. Wiley Environmental Molecular Sciences Laboratory (EMSL), a national scientific user facility sponsored by DOE's Office of Biological and Environmental Research and located at PNNL. PNNL is operated by Battelle for the DOE under Contract DE-AC05-76RLO1830. This work used the Extreme Science and Engineering Discovery Environment (XSEDE), which is supported by National Science Foundation grant number ACI-1053575. Neutron total scattering and PDF studies at ORNL's Spallation Neutron Source were sponsored by the Scientific User Facilities Division, Office of Basic Energy Sciences of the U.S. DOE.

■ REFERENCES

(1) Kim, S. W.; Seo, D. H.; Ma, X.; Ceder, G.; Kang, K. Electrode materials for rechargeable sodium-ion batteries: potential alternatives to current lithium-ion batteries. *Adv. Energy Mater.* **2012**, *2* (7), 710−721.

(2) Kundu, D.; Talaie, E.; Duffort, V.; Nazar, L. F. The emerging chemistry of sodium ion batteries for electrochemical energy storage. *Angew. Chem., Int. Ed.* **2015**, *54* (11), 3431−3448.

(3) Luo, W.; Shen, F.; Bommier, C.; Zhu, H.; Ji, X.; Hu, L. Na-ion battery anodes: materials and electrochemistry. *Acc. Chem. Res.* **2016**, *49* (2), 231−240.

(4) Pan, H.; Hu, Y.-S.; Chen, L. Room-temperature stationary sodium-ion batteries for large-scale electric energy storage. *Energy Environ. Sci.* **2013**, *6* (8), 2338−2360.

(5) Slater, M. D.; Kim, D.; Lee, E.; Johnson, C. S. Sodium-ion batteries. *Adv. Funct. Mater.* **2013**, *23* (8), 947−958.

(6) Wenzel, S.; Hara, T.; Janek, J.; Adelhelm, P. Room-temperature sodium-ion batteries: Improving the rate capability of carbon anode materials by templating strategies. *Energy Environ. Sci.* **2011**, *4* (9), 3342−3345.

(7) Nagaura, T.; Tozawa, K. Lithium ion rechargeable battery. *Prog. Batteries Sol. Cells* **1990**, *9*, 209.

(8) Jian, Z.; Luo, W.; Ji, X. Carbon Electrodes for K-Ion Batteries. *J. Am. Chem. Soc.* **2015**, *137* (36), 11566−11569.

(9) Luo, W.; Wan, J.; Ozdemir, B.; Bao, W.; Chen, Y.; Dai, J.; Lin, H.; Xu, Y.; Gu, F.; Barone, V. Potassium ion batteries with graphitic materials. *Nano Lett.* **2015**, *15* (11), 7671−7677.

(10) Fong, R.; Von Sacken, U.; Dahn, J. R. Studies of lithium intercalation into carbons using nonaqueous electrochemical cells. *J. Electrochem. Soc.* **1990**, *137* (7), 2009−2013.

(11) Mabuchi, A.; Tokumitsu, K.; Fujimoto, H.; Kasuh, T. Charge-discharge characteristics of the mesocarbon miocrobeads heat-treated at different temperatures. *J. Electrochem. Soc.* **1995**, *142* (4), 1041−1046.

DOI: 10.1021/acs.chemmater.6b05474
Chem. Mater. 2017, 29, 2314−2320

(12) Ohzuku, T.; Iwakoshi, Y.; Sawai, K. Formation of Lithium-Graphite Intercalation Compounds in Nonaqueous Electrolytes and Their Application as a Negative Electrode for a Lithium Ion (Shuttlecock) Cell. *J. Electrochem. Soc.* **1993**, *140* (9), 2490−2498.
(13) Asher, R.; Wilson, S. Lamellar compound of sodium with graphite. *Nature* **1958**, *181*, 409−410.
(14) Ge, P.; Fouletier, M. Electrochemical intercalation of sodium in graphite. *Solid State Ionics* **1988**, *28*, 1172−1175.
(15) Wen, Y.; He, K.; Zhu, Y.; Han, F.; Xu, Y.; Matsuda, I.; Ishii, Y.; Cumings, J.; Wang, C. Expanded graphite as superior anode for sodium-ion batteries. *Nat. Commun.* **2014**, *5*, 5.
(16) Nobuhara, K.; Nakayama, H.; Nose, M.; Nakanishi, S.; Iba, H. First-principles study of alkali metal-graphite intercalation compounds. *J. Power Sources* **2013**, *243*, 585−587.
(17) Azuma, H.; Imoto, H.; Yamada, S. i.; Sekai, K. Advanced carbon anode materials for lithium ion cells. *J. Power Sources* **1999**, *81*, 1−7.
(18) Luo, W.; Jian, Z.; Xing, Z.; Wang, W.; Bommier, C.; Lerner, M. M.; Ji, X. Electrochemically expandable soft carbon as anodes for Na-ion batteries. *ACS Cent. Sci.* **2015**, *1* (9), 516−522.
(19) Zhou, H.; Zhu, S.; Hibino, M.; Honma, I.; Ichihara, M. Lithium storage in ordered mesoporous carbon (CMK-3) with high reversible specific energy capacity and good cycling performance. *Adv. Mater.* **2003**, *15* (24), 2107−2111.
(20) Stevens, D.; Dahn, J. High capacity anode materials for rechargeable sodium-ion batteries. *J. Electrochem. Soc.* **2000**, *147* (4), 1271−1273.
(21) Li, Y.; Hu, Y. S.; Titirici, M. M.; Chen, L.; Huang, X. Hard Carbon Microtubes Made from Renewable Cotton as High-Performance Anode Material for Sodium-Ion Batteries. *Adv. Energy Mater.* **2016**, *6* (18), DOI: 10.1002/aenm.201600659.
(22) Li, Y.; Hu, Y.-S.; Li, H.; Chen, L.; Huang, X. A superior low-cost amorphous carbon anode made from pitch and lignin for sodium-ion batteries. *J. Mater. Chem. A* **2016**, *4* (1), 96−104.
(23) Qie, L.; Chen, W.; Xiong, X.; Hu, C.; Zou, F.; Hu, P.; Huang, Y. Sulfur-Doped Carbon with Enlarged Interlayer Distance as a High-Performance Anode Material for Sodium-Ion Batteries. *Adv. Sci.* **2015**, *2* (12), DOI: 10.1002/advs.201500195.
(24) Zhou, W.; Wang, S.; Li, Y.; Xin, S.; Manthiram, A.; Goodenough, J. B. Plating a Dendrite-Free Lithium Anode with a Polymer/Ceramic/Polymer Sandwich Electrolyte. *J. Am. Chem. Soc.* **2016**, *138* (30), 9385−9388.
(25) Jian, Z.; Xing, Z.; Bommier, C.; Li, Z.; Ji, X. Hard Carbon Microspheres: Potassium-Ion Anode Versus Sodium-Ion Anode. *Adv. Energy Mater.* **2016**, *6* (3), DOI: 150187410.1002/aenm.201501874.
(26) Mochida, I.; Korai, Y.; Ku, C.-H.; Watanabe, F.; Sakai, Y. Chemistry of synthesis, structure, preparation and application of aromatic-derived mesophase pitch. *Carbon* **2000**, *38* (2), 305−328.
(27) Guo, Y.; Shi, Z.-q.; Chen, M.-m.; Wang, C.-y. Hierarchical porous carbon derived from sulfonated pitch for electrical double layer capacitors. *J. Power Sources* **2014**, *252*, 235−243.
(28) Cao, B.; Liu, H.; Xu, B.; Lei, Y.; Chen, X.; Song, H. Mesoporous soft carbon as an anode material for sodium ion batteries with superior rate and cycling performance. *J. Mater. Chem. A* **2016**, *4* (17), 6472−6478.
(29) Franklin, R. E. Crystallite growth in graphitizing and non-graphitizing carbons. *Proc. R. Soc. London, Ser. A* **1951**, *209*, 196−218.
(30) Ding, J.; Wang, H.; Li, Z.; Kohandehghan, A.; Cui, K.; Xu, Z.; Zahiri, B.; Tan, X.; Lotfabad, E. M.; Olsen, B. C.; Mitlin, D. Carbon nanosheet frameworks derived from peat moss as high performance sodium ion battery anodes. *ACS Nano* **2013**, *7* (12), 11004−11015.
(31) Komaba, S.; Murata, W.; Ishikawa, T.; Yabuuchi, N.; Ozeki, T.; Nakayama, T.; Ogata, A.; Gotoh, K.; Fujiwara, K. Electrochemical Na insertion and solid electrolyte interphase for hard-carbon electrodes and application to Na-Ion batteries. *Adv. Funct. Mater.* **2011**, *21* (20), 3859−3867.
(32) Li, Z.; Ma, L.; Surta, T. W.; Bommier, C.; Jian, Z.; Xing, Z.; Stickle, W. F.; Dolgos, M.; Amine, K.; Lu, J. High Capacity of Hard Carbon Anode in Na-Ion Batteries Unlocked by PO x Doping. *ACS Energy Lett.* **2016**, *1* (2), 395−401.
(33) Jian, Z.; Zhao, L.; Pan, H.; Hu, Y.-S.; Li, H.; Chen, W.; Chen, L. Carbon coated Na 3 V 2 (PO 4) 3 as novel electrode material for sodium ion batteries. *Electrochem. Commun.* **2012**, *14* (1), 86−89.
(34) Padhi, A. K.; Nanjundaswamy, K.; Goodenough, J. Phospho-olivines as positive-electrode materials for rechargeable lithium batteries. *J. Electrochem. Soc.* **1997**, *144* (4), 1188−1194.
(35) Bommier, C.; Ji, X. Recent Development on Anodes for Na-Ion Batteries. *Isr. J. Chem.* **2015**, *55* (5), 486−507.
(36) Dmowski, W.; Contescu, C. I.; Llobet, A.; Gallego, N. C.; Egami, T. Local atomic density of microporous carbons. *J. Phys. Chem. C* **2012**, *116* (4), 2946−2951.
(37) Fu, L.; Tang, K.; Song, K.; van Aken, P. A.; Yu, Y.; Maier, J. Nitrogen doped porous carbon fibres as anode materials for sodium ion batteries with excellent rate performance. *Nanoscale* **2014**, *6* (3), 1384−1389.
(38) Kresse, G.; Hafner, J. Ab initio molecular dynamics for liquid metals. *Phys. Rev. B: Condens. Matter Mater. Phys.* **1993**, *47* (1), 558.
(39) Kresse, G.; Hafner, J. Ab initio molecular-dynamics simulation of the liquid-metal−amorphous-semiconductor transition in germanium. *Phys. Rev. B: Condens. Matter Mater. Phys.* **1994**, *49* (20), 14251.
(40) Kresse, G.; Furthmüller, J. Efficient iterative schemes for ab initio total-energy calculations using a plane-wave basis set. *Phys. Rev. B: Condens. Matter Mater. Phys.* **1996**, *54* (16), 11169.
(41) Blöchl, P. E. Projector augmented-wave method. *Phys. Rev. B: Condens. Matter Mater. Phys.* **1994**, *50* (24), 17953.
(42) Kresse, G.; Joubert, D. From ultrasoft pseudopotentials to the projector augmented-wave method. *Phys. Rev. B: Condens. Matter Mater. Phys.* **1999**, *59* (3), 1758.
(43) Perdew, J. P.; Burke, K.; Ernzerhof, M. Generalized gradient approximation made simple. *Phys. Rev. Lett.* **1996**, *77* (18), 3865.
(44) Grimme, S.; Antony, J.; Ehrlich, S.; Krieg, H. A consistent and accurate ab initio parametrization of density functional dispersion correction (DFT-D) for the 94 elements H-Pu. *J. Chem. Phys.* **2010**, *132* (15), 154104.
(45) Grimme, S.; Ehrlich, S.; Goerigk, L. Effect of the damping function in dispersion corrected density functional theory. *J. Comput. Chem.* **2011**, *32* (7), 1456−1465.
(46) Monkhorst, H. J.; Pack, J. D. Special points for Brillouin-zone integrations. *Phys. Rev. B* **1976**, *13* (12), 5188.

DOI: 10.1021/acs.chemmater.6b05474
Chem. Mater. 2017, 29, 2314−2320